J. Appl. Comput. Mech., 7(1) (2021) 372-381
DOI: 10.22055/JACM.2020.35128.2571

ISSN: 2383-4536
jacm.scu.ac.ir

Shahid Chamran University of Ahvaz

Journal of Applied and Computational Mechanics

Research Paper

A Case Study of Combined Application of Smart Materials in a Thermal Energy Harvester with Vibrating Action

Rosen Mitrev[1], Todor Todorov[2], Andrei Fursov[3], Vasily Fomichev[4], Alexander Il'in[5]

[1] Department of Logistics Engineering, Material Handling and Construction Machines, Mechanical Engineering Faculty, Technical University of Sofia, Sofia, 1797, Bulgaria, Email: rosenm@tu-sofia.bg

[2] Department of Theory of Mechanisms and Machines, Faculty of Industrial Technology, Technical University of Sofia, Sofia, 1797, Bulgaria, Email: tst@tu-sofia.bg

[3,4,5] Department of Nonlinear Dynamical Systems and Control Processes, Faculty of Computational Mathematics and Cybernetics, Lomonosov Moscow State University, Moscow, 119991, Russia, Email: fursov@cs.msu.ru, fomichev@cs.msu.ru, iline@cs.msu.ru

Received September 21 2020; Revised October 17 2020; Accepted for publication October 26 2020.
Corresponding author: Rosen Mitrev (rosenm@tu-sofia.bg)

Abstract. This paper demonstrates a case study of a combined application of smart materials in a thermal energy harvester with vibrating action. The conceptual design of the harvester is based on a Shape Memory Alloy wire attached to the free end of a piezoelectric flexible cantilever beam intended for generation of electrical energy utilizing a constant heat source. A mathematical model containing three differential equations describing the dynamics of the mechanical, electrical and thermal subsystems is developed. The Shape Memory Alloy hysteretic behaviour is considered in the mathematical model. An essential observation is the system oscillates at two frequencies lower one of which depends on the temperature time constant and the higher one is determined by the natural frequency of the mechanical subsystem. The comparison of the numerical solutions and the experimentally obtained graphs of the harvester output characteristics shows a good degree of coincidence.

Keywords: Thermal energy harvester, Smart materials, Vibration.

1. Introduction

Over the last decades, considerable attention has been paid to the problem of waste energy use. A significant amount of research has been done on collecting energy from the environment and converting it into electrical energy through energy harvesters of different types. The collection of waste thermal energy represents a promising and cost-effective direction, which is developing more intensively compared to the utilization of other types of energy. Mainly, technical devices with two operational principles are employed. The first principle is based on the direct conversion of the thermal energy into electrical one while the second principle uses an intermediate conversion of the thermal energy into mechanical, followed by a conversion of the mechanical energy into electrical.

The direct transformation of the thermal into electrical energy is based on various physical effects [1] with different efficiency. The thermionic conversion is a physical phenomenon of spontaneous ejection of electrons from a hot surface [2], the pyroelectric converters are based on the generation of the electrical potential in some crystals when they are heated or cooled [3] and the Seebeck semiconductor thermoelectric generators directly convert the temperature difference into a voltage potential [4]. The alkali metal thermal-to electric converters employ the properties of the beta alumina solid electrolyte to conduct sodium ions [5]. The Johnson thermo-electrochemical converter utilizes a pressure differential formed by the heat drive of the positive ions [6].

The fundamental principles for the transformation of thermal-to mechanical-to electrical energies are also relatively diverse. At the first stage, the conversion of the thermal to mechanical energy is based primarily on the use of the well-known thermomechanical heat engines using different thermodynamic cycles [7-9]. Thermomechanical systems based on different physical principles are also utilized. Travelling and standing waves thermoacoustic engines use heat to efficiently generate oscillating acoustic waves within a working fluid [10,11]. The phenomenon of the change of the magnetization of some materials under the influence of temperature change is exploited in the thermomechanical motors [12,13]. Hydride heat engines utilize the property of some unique alloys to store and release hydrogen within their crystal lattice [1].

Shape memory alloys (SMA) based engines and actuators are utilized for many practical purposes in diverse areas like power systems, civil structures and medicine [14-17]. Their operational principle is based on the ability to regain their shape under the influence of heat. This effect results from the change of the crystallographic structure of the SMA when the temperature changes [18] and it is widely used for actuation applications and mechanical energy transformation. Depending on the application, the academic researchers and engineers have developed SMA actuators with continuous [19] and oscillating motion [20].

Published online: November 09 2020

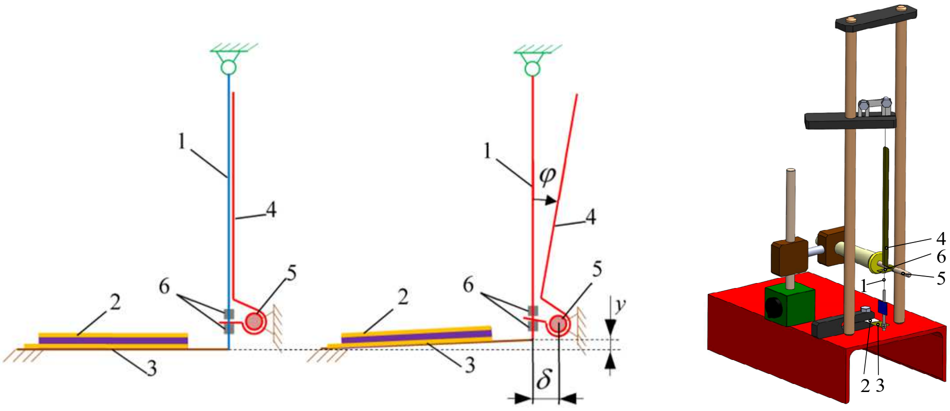

Fig. 1. Kinematical scheme of the SMA-PETEH: (a) for cold SMA wire; (b) for heated SMA wire; (c) schematic configuration

The second stage mechanical-to-electrical conversion uses the well-studied piezoelectric, magnetic, electrostatic, triboelectric [21] and elastoelectric converters as well as novel operating principles [22]. Combining different physical principles and smart materials a broad variety of hybrid energy harvesters is already designed and studied. The authors of [23] present Piezo-SMA based thermal energy harvester modelled by 1D serial model and the 3D model with the Eshelby theory. The paper [24] presents a hybrid actuation and energy harvesting system consisting of a piezoelectric bimorph and a SMA wire heated by a laser. Another unusual device to utilize the solar energy and consisting of piezoelectric cantilever beam and SMA spring actuator is presented in [25]. Todorov et al. [26] demonstrated the concept of smart materials combination in the developed novel type of thermoelectric energy harvester with thermally induced vibrations in a SMA wire through a heater with constant heat. A novel dynamical model is presented assuming small vibrations and neglecting the hysteresis in the SMA wire. The design and control of the combined devices are considerably facilitated by the recently developed numerical tools for FE modelling of smart material based active elements embedded in structures [27-30].

The present paper aims to develop, study and validate a nonlinear mathematical model of an energy harvester of the type thermal-to mechanical – to electrical energy combining piezoelectric cantilever beam and SMA wire considering the hysteretic behaviour of the SMA.

2. Design of a Shape Memory Alloy Piezoelectric Thermal Energy Harvester

Figure 1a) depicts the kinematical scheme of the designed Shape Memory Alloy piezoelectric thermal energy harvester (SMA-PETEH) [26] and Figure 1c) shows the schematic configuration of the device. Its operational principle is based on the repeated deformation of a piezoelectric layer due to the force action of a SMA wire subjected to sequential heating and cooling. The free end of the deformed cantilever beam 3 with deposited piezoelectric layer 2 stretches the vertically arranged SMA wire 1. The heated by the heater 5 brass plate 4 contacts lengthwise the wire also heated. Figure 1b) shows the layout of the SMA-PETEH with heated SMA wire which has undergone crystallographic changes due to the heating. The heating leads to a transition from martensite to austenite structure resulting in a shortening of the wire causing an upward movement of the beam free end. The resulting deformation of the piezoelectric layer generates an electrical charge. Due to the presence of the stops 6, the shortening of the wire causes a clockwise rotation of the plate, leading to its distancing from the wire which begins to cool. Another austenite to martensite transformation decreases the SMA wire stiffness, and it lengthens under the influence of the cantilever beam force. The plate rotates counterclockwise whereat cantilever beam deforms again and the piezoelectric layer generates a second portion of electrical charge. The described process exhibits periodic behaviour with a certain frequency determined by the system parameters.

3. Mathematical Modelling of the System

3.1 Modelling of the SMA wire force

The mechanical properties of the SMA wire depend on its temperature and stress. At low temperature, the SMA has twinned or detwinned martensite structure correspondingly for low and high stress. At high temperature, the SMA has an austenite structure and the transition between the two phases is accomplished by mixed structures consisting of both phases in different proportions. The ratio

$$R_m = \frac{V_M}{V} \tag{1}$$

of the volume of the martensite V_m to the entire volume V of SMA is called martensite fraction. Many mathematical models describing the hysteretic behaviour of the SMA [31,32] are based on the temperature dependence of the martensite fraction value. Unlike the models used so far, in this paper the martensite fraction is presented by the following equation:

$$R_m = 0.5\left(1 + \tanh\frac{T_m - T}{k_T}\right) \tag{2}$$

where the following notations are used:

$$T_m = \begin{cases} 0.5\left(A_s + A_f\right) & if\ \ \dot{T} > 0 \\ 0.5\left(M_s + M_f\right) & if\ \ \dot{T} < 0 \end{cases} \tag{3}$$

$$k_T = \begin{cases} \dfrac{A_f - A_s - 2b_a}{2c_a} & if\ \dot{T} > 0 \\ \dfrac{M_s - M_f - 2b_m}{2c_m} & if\ \dot{T} < 0 \end{cases} \tag{4}$$

A_s and A_f are the start and the final austenite temperatures; M_s and M_f are the start and the final martensite temperatures; $b_a < 0.5(A_f - A_s)$, $b_m < 0.5(M_s - M_f)$, $c_a < 0.5$, $c_m < 0.5$ are experimentally determined constants; T is the temperature of the wire. Figure 2 shows the graph of the martensite fraction plotted by the use of Eqs. (2) ÷ (4).

By the use of Eqs. (2) ÷ (4) the force produced by the SMA wire is presented as a function of its deformation ε_s by the following piecewise function:

$$F_s = \begin{cases} (E_a - (E_a - E_m)R_m)\varepsilon_s A_w, & if\quad 0 \le \varepsilon_s \le \varepsilon_m^y \\ (E_a - (E_a - E_T)R_m)\varepsilon_s A_w - (E_T - E_m)\varepsilon_m^y R_m A_w, & if\quad \varepsilon_m^y \le \varepsilon_s \le \varepsilon_m^d \\ (E_a - (E_a - E_d)R_m)\varepsilon_s A_w - (E_T - E_m)R_m\varepsilon_m^y A_w - (E_d - E_T)R_m\varepsilon_m^d A_w, & if\quad \varepsilon_m^d \le \varepsilon_s \end{cases} \tag{5}$$

where E_m, E_T, E_d, and E_a are Young's modulus of the fully twined, partially twined, detwinned martensite and austenite respectively; ε_m^y is the yield strain of the twined martensite; ε_m^d is the minimum strain of the detwinned martensite; A_w is the cross-sectional area of the SMA wire. In Fig. 3 is shown the graph of the SMA wire force for a constant temperature of 39 °C. Position 1 designates the graph of the force for decreasing temperature (cooling) and position 2 designates the graph of the force for increasing temperature (warming).

3.2 Determination of the initial deformations and positions

The piezoelectric cantilever beam and SMA wire deformations are considered as shown in Figure 4 [26]. In the free undeformed state (before the connection), the longitudinal axis of the cantilever beam is a straight line denoted by *CD* and the initial length of the SMA wire is denoted by *AE*.

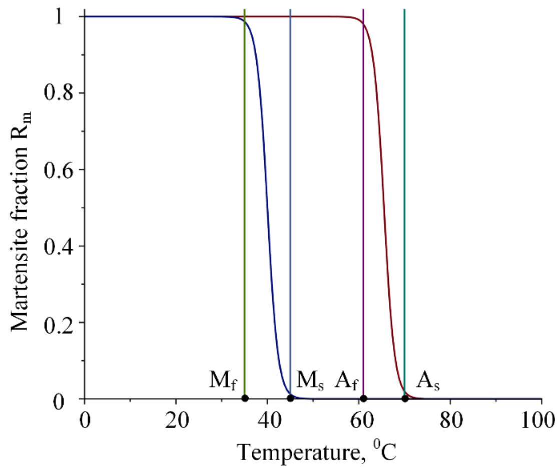

Fig. 2. Martensite fraction R_m expressed by the hyperbolic tangent function

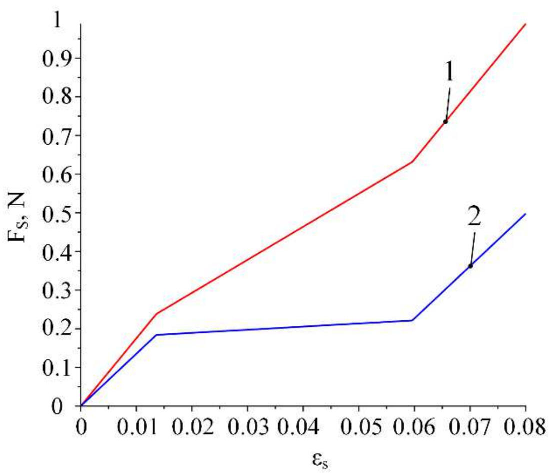

Fig. 3. SMA wire force for a constant temperature of 39 °C: 1 – cooling, 2 – warming

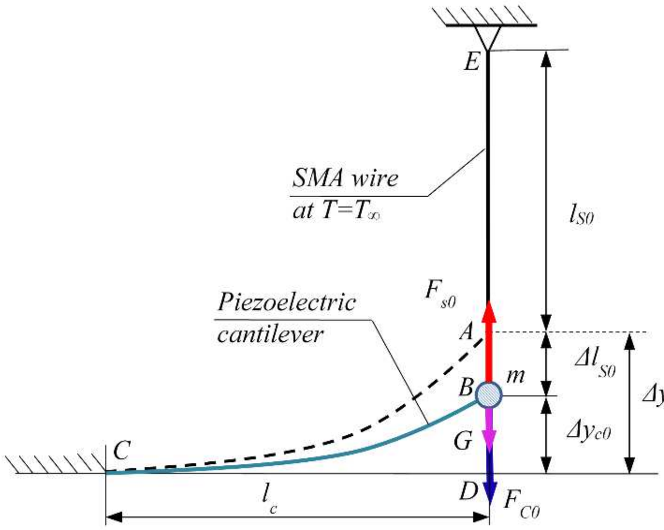

Fig. 4. Deformations of the SMA wire and the piezoelectric cantilever beam

The following designations are used when the free end of the cantilever beam (point *D*) is connected to the wire end (point *A*): 1) if the deformation of the wire is not considered than Δy_0 is the deformation of the free end of the beam and l_{S0} is the SMA wire length; 2) if the deformation of the SMA wire is taken into account the equilibrium position of the system is at the point *B* and Δy_{c0} is the deformation of the free end of the cantilever beam and Δl_{S0} is the SMA wire deformation. The force F_{c0} acting at the free beam end is:

$$F_{c0} = k_c \Delta y_{c0} \tag{6}$$

where

$$k_c = \frac{3E_c I}{l_c^3} \tag{7}$$

is the stiffness of the cantilever beam; E_c is the Young modulus of the beam material; l_c is the length of the beam. The moment of inertia of the beam section is $I = wh^3/12$, where w and h designate the width and the thickness of the beam section. According to [32], the SMA wire equilibrium force F_{S0} is:

$$F_{s_0} = \begin{cases} E_m A_w \varepsilon_{s_0} & \text{if} \quad \varepsilon_{s_0} < \varepsilon_m^y \\ \Delta E_{mT} A_w \varepsilon_m^y + E_T A_w \varepsilon_{s_0} & \text{if} \quad \varepsilon_m^y \le \varepsilon_{s_0} \le \varepsilon_m^d \\ \Delta E_{mT} A_w \varepsilon_m^y + \Delta E_{Td} A_w \varepsilon_{s_1} + E_d A_w \varepsilon_{s_0} & \text{if} \quad \varepsilon_m^d \le \varepsilon_{s_0} \end{cases} \tag{8}$$

where the differences of Young's modules are denoted by $\Delta E_{mT} = E_m - E_T$, $\Delta E_{Td} = E_T - E_d$.

It is assumed that at the point *B* acts the weight *G* of the generalized mass *m*:

$$G = mg \tag{9}$$

The static equilibrium of the forces F_{C0}, F_{S0} and *G* is expressed by the following equation:

$$k_c \Delta y_{c0} + mg = F_{s0} \tag{10}$$

Also, from Fig. 4 it follows the geometric condition:

$$\Delta y_0 = \Delta l_{S0} + \Delta y_{c0} \tag{11}$$

Substituting in eq. (11) the initial deformation of the SMA wire Δl_{S0} with

$$\Delta l_{S0} = l_{S0} \varepsilon_{s_0} \tag{12}$$

and solving the equations (10) and (11) as a system, expressions for the unknown values of Δy_{c0} and ε_{S0} are obtained:

$$\varepsilon_{s_0} = \begin{cases} \dfrac{k_c \Delta y_0 + mg}{E_m A_w + k_c l_{S0}} & \text{if} \quad \varepsilon_{s_0} < \varepsilon_m^y \\ \dfrac{k_c \Delta y_0 + mg - \varepsilon_m^y A_w \Delta E_{mT}}{E_T A_w + k_c l_{S0}} & \text{if} \quad \varepsilon_m^y \le \varepsilon_{s_0} \le \varepsilon_m^d \\ \dfrac{k_c \Delta y_0 + mg - \varepsilon_m^d A_w \Delta E_{Td} - \varepsilon_m^y A_w \Delta E_{mT}}{E_d A_w + k_c l_{S0}} & \text{if} \quad \varepsilon_m^d \le \varepsilon_{s_0} \end{cases} \tag{13}$$

$$\Delta y_{c0} = \begin{cases} \dfrac{A_w E_m \Delta y_0 - l_{S0} mg}{E_m A_w + k_c l_{S0}} & if\ \varepsilon_{s_0} < \varepsilon_m^y \\ \dfrac{A_w\left(\Delta E_{mT} l_{S0} \varepsilon_m^y - E_T \Delta y_0\right) - l_{S0} mg}{E_T A_w + k_c l_{S0}} & if\ \varepsilon_m^y \le \varepsilon_{s_0} \le \varepsilon_m^d \\ \dfrac{A_w\left(\Delta E_{Td} l_{S0} \varepsilon_m^d + E_{mT} l_{S0} \varepsilon_m^y + E_d \Delta y_0\right) - l_{S0} mg}{E_d A_w + k_c l_{S0}} & if\ \varepsilon_m^d \le \varepsilon_{s_0} \end{cases} \tag{14}$$

To avoid the penetration of the plate into the SMA wire the plate rotation angle *φ(y)* is constrained to positive values:

$$\varphi(y) = \begin{cases} \arctan\dfrac{y}{\delta} & if\ \ y > 0 \\ 0 & if\ \ y \le 0 \end{cases} \tag{15}$$

where: y is the deflection of the cantilever beam free end; δ is the distance between the SMA wire and the axis of the rotation of the hot plate (see Fig. 1).

The temperature transferred from the hot plate to the SMA wire is modelled by the following relationship:

$$T_{hp} = \begin{cases} T_\infty + \dfrac{T_h}{2k_{Th}}\left(1 + \cos\dfrac{\pi\varphi(y)}{\varphi_m}\right) & if\ \ \varphi(y) < \varphi_m \\ T_\infty & if\ \varphi(y) \ge \varphi_m \end{cases} \tag{16}$$

where the following notations are used: T_{hp} is the temperature transferred from the hot plate to the SMA wire; T_h is the temperature of the hot plate; φ_m is the maximum angle of rotation of the hot plate; T_∞ is the temperature of the room; k_{Th} is an experimentally determined constant.

Due to the one-way action of the SMA wire, the damping coefficient is defined as a function of y:

$$\beta = \begin{cases} \beta_c + \beta_{SMA} & if\ y < \Delta y_{c0} + \Delta l_{S0} \\ \beta_c & if\ y \ge \Delta y_{c0} + \Delta l_{S0} \end{cases} \tag{17}$$

where β_{SMA} and β_c are the damping coefficients of the SMA wire and the cantilever beam correspondingly.

3.3 Dynamical modelling

The behaviour of the SMA-PETEH is determined by the dynamics of the constituent subsystems belonging to different physical domains - mechanical, electrical, and thermal. The mutual interaction between the subsystems is illustrated by the simplified diagram shown in Fig. 5. The mechanical subsystem is presented as a generalized mass concentrated at the point *B* whose position y is considered as a mechanical generalized coordinate. The electrical subsystem consists of a piezoelectric transducer C_p and a loading resistor R_L and the charge *q* is chosen as an electrical generalized coordinate. The thermal subsystem is presented by its equivalent electrical circuit shown in Fig. 5 where the following notations are used: LT_{hp} is the equivalent thermal inductance, RT_{SMA} is the nonlinear equivalent thermal resistor, which depends on the thermal conductivity α_s, RT_r is the equivalent thermal resistor depending on heat convective transfer coefficient, and Q_h is the equivalent thermal voltage.

The generalized coordinate for this equivalent circuit is:

$$\lambda_T = \int_0^t T dt \tag{18}$$

The Lagrangian for the entire multiphysical system is defined as:

$$W_L = W_K - W_\Pi - W_{PT} + W_T \tag{19}$$

In eq. (19) the following notations are used:

$$W_k = \frac{m\dot{y}^2}{2} \tag{20}$$

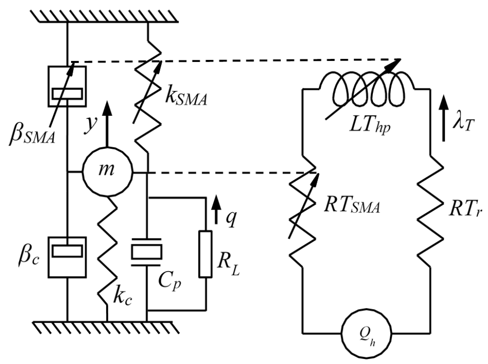

Fig. 5. The dynamical model of the energy harvester

is the kinetic energy of the system;

$$W_{\Pi} = \frac{ky^2}{2} \tag{21}$$

is the potential energy of the system;

$$W_{PT} = \frac{q^2}{2C\left(1-k_p^2\right)} - \frac{d_{33}K_a}{C\left(1-k_p^2\right)}q\Delta + \frac{K_a}{1-k_p^2}\frac{\Delta^2}{2} \tag{22}$$

is the piezoelectric energy according to [34]. In (22) the following notations are used: k_p^2 is the electromechanical coupling coefficient of the piezoelectric layer and

$$\Delta = p_y y \tag{23}$$

is the longitudinal deformation of the piezoelectric layer; p_y is the coupling coefficient between longitudinal deformation and the displacement of the cantilever beam free end along axis y as explained in [34]. The equivalent capacitance C is:

$$C = \frac{\varepsilon w_p\left(l_p + p_y y\right)}{g_p} \tag{24}$$

where ε is the piezoelectric permittivity of PZT; w_p, l_p and g_p are the width, length, and thickness of the piezoelectric layer. In (22) d_{33} is the piezoelectric constant; $K_a = 3I_p/s^E l_p^3$, s^E is the compliance when the electric field is constant; I_p is the moment of inertia of the piezoelectric layer section; t is the time;

$$W_T = \frac{LT_{hp}\lambda_T^2}{2} \tag{25}$$

is the thermal energy where $LT_{hp} = \rho_s A_w c_p$; ρ_s and c_p are the density and the specific heat of the NiTi alloy.

Based on the above assumptions the dynamical model of the system obtains the following form:

$$\left|\begin{array}{l} m\dfrac{d^2y}{dt^2} + \beta\dfrac{dy}{dt} + k_c y - \dfrac{C'}{2C^2\left(1-k_p^2\right)}q^2 + \dfrac{d_{33}K_a p_y C'}{C^2\left(1-k_p^2\right)}qy - \dfrac{d_{33}K_a p_y}{C\left(1-k_p^2\right)}q + \dfrac{K_a p_y}{\left(1-k_p^2\right)}y = F_s \\ \rho_s A_w c_p\dfrac{dT}{dt} = h_c A_o(T_\infty - T) + \alpha_s A_c\left(T_{hp}\varphi(y) - T\right) \\ \dfrac{1}{C\left(1-k_p^2\right)}q + \dfrac{d_{33}K_a p_y}{C\left(1-k_p^2\right)}y = -R_L\dot{q} \end{array}\right. \tag{26}$$

where C' is the derivative of C with respect to y; h_c is the heat convective transfer coefficient; A_o is the circumferential area per unit length of the SMA wire; A_c is the contact area per unit length between the wire and hot plate; F_s is the SMA wire force, determined according to Eq. (5). The thermal conductivity between the SMA wire and the plate is:

$$\alpha_s = \alpha_{sA} + \left(\alpha_{sM} - \alpha_{sA}\right)R_m(T) \tag{27}$$

where α_{sA} and α_{sM} are the thermal conductivity between nitinol and brass at austenite and martensite phases respectively (see Table I).

The first equation in the system (26) represents the balance of the forces in y-direction, the second equation represents the temperature behaviour of the energy harvester, and the third equation represents the balance of the voltages.

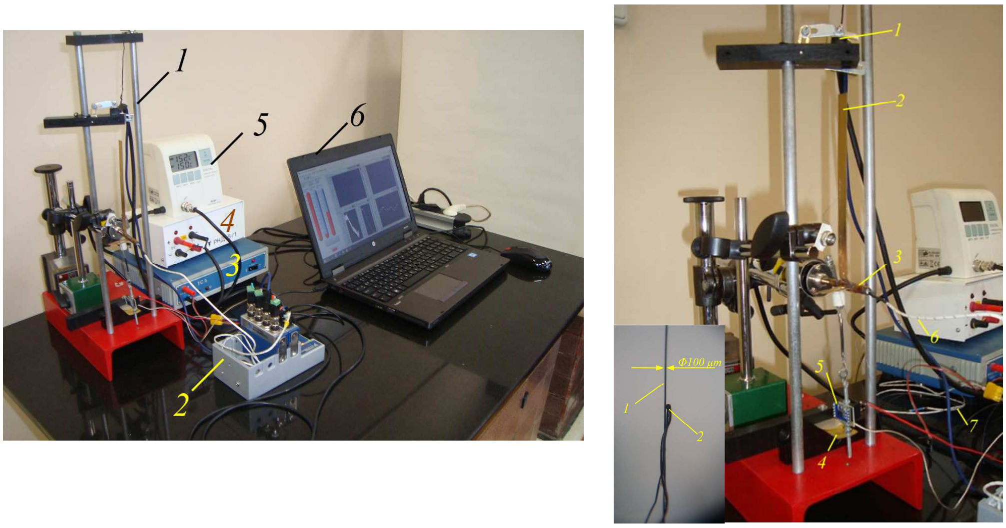

(a) (b)

Fig. 6. A layout view of the experimental setup and sensors placement

Table 1. Numerical values of the model parameters.

Symbol	Quantity	Value and unit
m	Generalized mass	0.0023 kg
k_c	Cantilever beam stiffness	86.4 N/m
E	Young's modulus of the cantilever beam	0.11×10^{12} Pa
l	Length of the cantilever beam	0.032 m
w	Width of the cantilever beam	0.018 m
h	Thickness of the cantilever beam	0.0004 m
l_p	Length of the piezoelectric layer	0.016 m
ε_{33}	Permittivity of PZT-5H	1.24×10^{-8} F/m
d_{33}	Piezoelectric constant of PZT-5H	590×10^{-12} C/N
h_p	Thickness of the piezoelectric layer	0.0003 m
δ	Distance between the SMA wire and center of rotation of the plate	0.003 m
K_a	Stiffness of the piezoelectric layers at shortcut electrodes	30.52 N/m
k_p	Electromechanical coupling coefficient	0.75
s^E	Compliance of PZT-5H at constant electric field	2×10^{-11} Pa^{-1}
β	Coefficient of viscous resistance	0.002 kg/s
R_L	Loading resistor	10×10^6 Ω
s_0	Initial length of the SMA wire	0.244 m
ρ_s	Density of the SMA wire	6450 kg/m3
d_s	Diameter of the SMA wire	0.00001 m
α_{sM}	Thermal conductivity of NiTi at martensite phase	18 W/(m °C)
α_{sA}	Thermal conductivity of NiTi at austenite phase	8.6 W/(m °C)
h_c	Heat transfer coefficient between air and NiTi	70 W/(m2 °C)
k_{Th}	Temperature approximation coefficient	1.2
c_p	Specific heat	836 J/(kg·°C)
c_m	First approximation coefficient for martensite state	2.17 °C
c_a	First approximation coefficient for austenite state	1.95 °C
b_m	Second approximation coefficient for martensite state	0.01 °C
b_a	Second approximation coefficient for austenite state	0.01 °C
T_h	Temperature of the heater	120 °C
T_∞	Temperature of the room	20 °C
M_s	Start martensite temperature	45 °C
M_f	Final martensite temperature	35 °C
A_s	Start austenite temperature	61 °C
A_f	Final austenite temperature	70 °C
E_a	Young's modulus of NiTi at austenite	3.44×10^9 Pa
E_T	Young's modulus of NiTi at partly twinned martensite	1.03×10^9 Pa
E_d	Young's modulus of NiTi at detwinned martensite	1.72×10^9 Pa
E_m	Young's modulus of NiTi at fully twined martensite	1.72×10^9 Pa
ε_m^y	Yield strain of twined martensite	0.0136
ε_m^d	Minimum strain of detwinned martensite	0.0596
φ_m	Maximum angle of the plate	15 deg

4. Numerical Solutions and Validation of the Mathematical Model

In Figure 6 is shown the view of the produced experimental setup for the examination of the designed SMA-PETEH behaviour. It consists of the following basic elements shown on the general view in Figure 6 a): 1 –Experimental setup; 2 – DAQ; 3, 4 – Rectifiers; 5 – Thermal regulator; 6 – Computer. The layout of the used sensors is shown in Figure 6 b): 1 - Piezoresistive force sensor 1 of type FSG15N1A for measurement the longitudinal force in the SMA wire; 2 - Brass hot plate; 3 – Heater; 4 – Piezoelectric cantilever beam; 5 - Three-axis accelerometer 5 of type ADXL345 measuring the acceleration of the cantilever beam along the vertical axis (y-coordinate); 6 – Thermocouple for measuring the heater temperature; 7- Thermocouple for measuring the room temperature. For the improvement of the dynamics of the temperature measurement of the SMA wire, a type-T thermocouple with a diameter of 100 µm is used (shown in the lower-left corner of Figure 6 b), 1 – SMA wire, 2 – Thermocouple). The sensor analog outputs are processed by a National Instruments cDAQ-9174 compact DAQ Chassis and modules Ni9201, Ni9229 and Ni9211. Labview software for the initial data processing and visualization is used.

The system of eqs. (26) is solved numerically by the implicit Euler method using the numerical values shown in Table 1. Initial conditions for the variables are: $y(0)=0$, $\dot{y}(0)=0$, $T(0)=T_\infty$. At time t=0 the charge q has a value, computed from the third equation of (26) for $\dot{q}=0$:

$$q(0)=-d_{33}K_a p_y y(0) \tag{28}$$

The presented here experimental setup is used to conduct a series of experiments for obtaining the graphs of some system output characteristics and compare them to the numerical solutions. Figure 7 presents the numerical solutions overlapped with the experimental results.

In Fig. 7a) are shown the numerical 1 and the experimental 2 graphs for the SMA wire force. As one can see, the force has periodic stable behaviour and two types of motions with different frequencies are present in the graph. The first one has a value of 4 Hz as can be concluded from the filtered force graph denoted by pos.3. This motion is caused by the temperature phase transitions in the SMA wire accompanied by its lengthening and shortening and the value of the frequency depends on the temperature time constant τ of the thermal subsystem [33]:

$$\tau=\rho_s A_w c_p\left(\frac{1}{h_c A_o}+\frac{1}{\alpha_s A_c}\right) \tag{29}$$

Except the temperature-dependent frequency, there exists another one motion with a higher frequency with value about 46 Hz. It is modulated by the temperature-dependent frequency and its value is equal to the natural frequency ω_S of the mechanical subsystem:

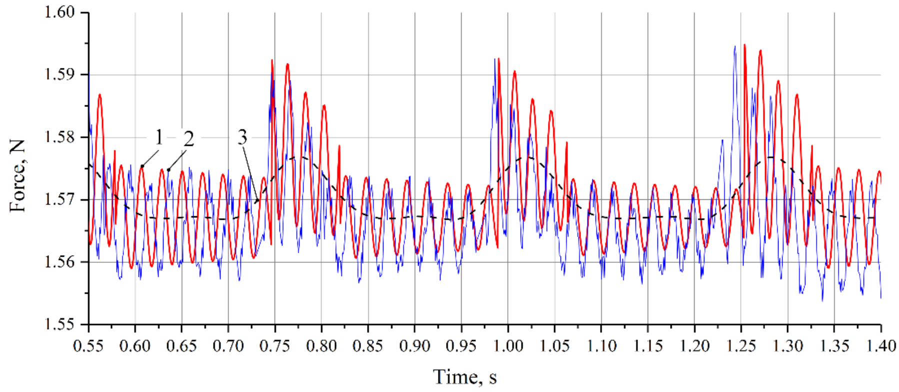

(a)

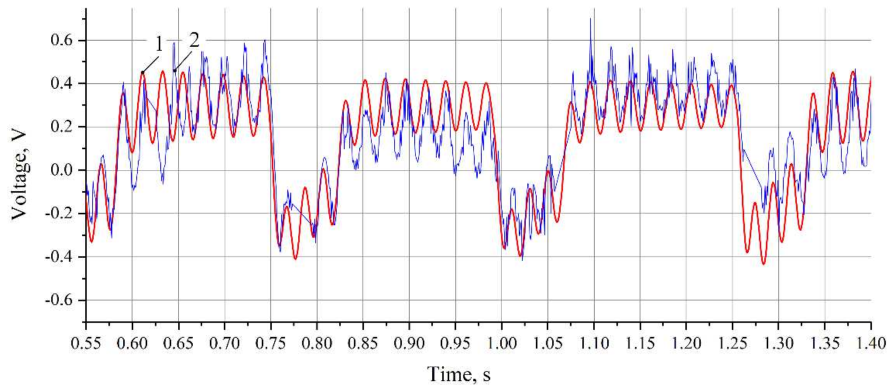

(b)

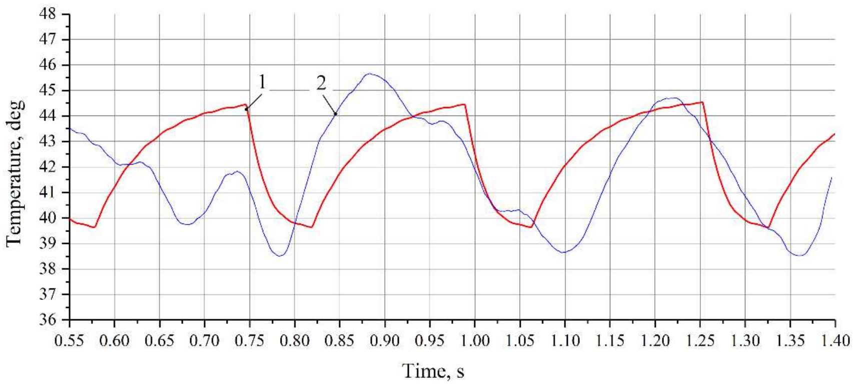

(c)

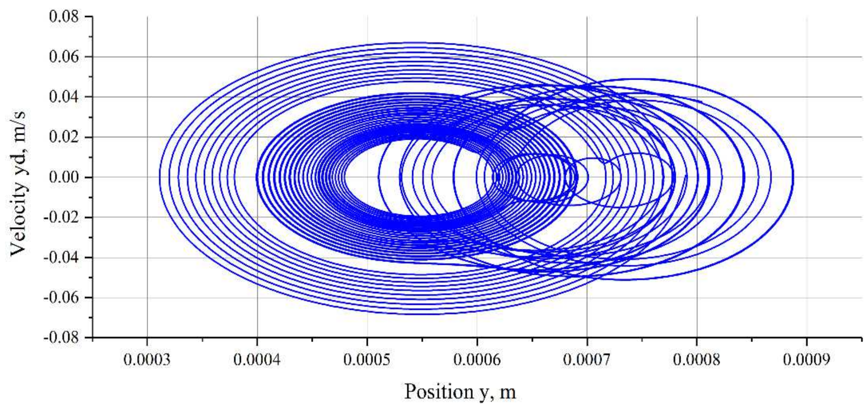

(d)

Fig. 7. Graphs of the system output characteristics for the steady-state: a) Force in the SMA wire; b) Generated voltage by the piezoelectric transducer; c) Temperature of the SMA wire; d) Phase trajectory of the point mass

$$\omega_S = \sqrt{\frac{k_c + k_{SMA}}{m}} \tag{30}$$

where

$$k_{SMA} = \frac{E(T)A_w}{l_{S0}} \tag{31}$$

is the SMA wire stiffness and Young's modulus is:

$$E(T) = \frac{F_s}{A_w \varepsilon_s} \tag{32}$$

The equation (30) hints that the stiffness change of the SMA wire causes an additional frequency modulation, but it is weakly expressed on the theoretical and experimental graphs.

In Figure 7b) are shown numerically 1 and experimentally 2 obtained graphs of the voltage, generated by the piezoelectric layer. It is also periodic with a frequency determined by the two mentioned frequencies. The maximal value of the voltage is about 0.6 V. Figure 7c) depicts numerically 1 and experimentally 2 obtained graphs of the SMA wire temperature. The smoothly rising section of the temperature corresponds to the heating when the heater is approaching the wire followed by a descending section when cooling. The change of the wire temperature is between 39°C and 46°C. The main reason for the incomplete coincidence between the numerical solution and the experimental curve is the high-temperature inertia of the thermocouple used. In Fig. 7d) is shown the phase trajectory of the point mass. As it is confirmed by the other graphs, there are vibrations of the mass with variable amplitude around two equilibrium positions. The maximum displacement and velocity of the mass are about 0.9 mm and 0.07 m/s correspondingly.

An additional parametric study showed a large sensitivity of the output characteristics and a rich variety of dynamic regimes which is a premise for optimization of the system. Moreover, conditions for the existence of oscillatory modes in the system are established in [35].

The comparison between the presented numerical and experimental curves shows a satisfactory coincidence between the amplitudes, shapes and frequencies for the depicted output characteristics. The main reason for the observed differences is the approximate character of the developed mathematical model and the presence of uncertainty for the values of some constants.

The higher efficiency of the energy harvester could be obtained if the frequencies of the mechanical and the thermally-induced oscillations coincide. For the considered case the mechanical frequency is about 10 times bigger than the thermal frequency. The coincidence of the frequencies requires an increase of the circumferential area and a decrease of the volume per unit length of the SMA wire. A successful design approach would be the reduction of the size of the device which will increase the mechanical and thermal frequencies but with different scale factors allowing their equalization or at least approaching each other. This approach shows that the miniaturization of the developed energy harvester improves its performance.

5. Conclusions

This paper studied problems related to the combined application of smart materials in a thermal energy harvester with vibrating action. The development and investigation of a thermal energy harvester whose operational principle is based on the deformation of a piezoelectric cantilever beam through repeatedly heated and cooled SMA wire employing a constant heat source.

A mathematical model of the system composed of equations from mechanical, thermal and electrical domains is developed and numerically solved. The SMA wire force model takes into account the SMA hysteretic behaviour. It was found that the system oscillates at two main frequencies – a lower one, determined by the temperature time constant of the system and a higher one, determined by the natural frequency of the mechanical subsystem. The experimental validation performed shows a relatively good coincidence between the theoretical and experimental results therefore it can be confirmed that the mathematical model describes with sufficient accuracy the dynamic behavior of the studied system. Some conclusions and directions for improving the harvester output characteristics have been formulated.

The following goal is to maximize harvested energy and to optimize the geometrical design of the device.

Author Contributions

R. Mitrev and T. Todorov planned the scheme, developed the mathematical modeling and conducted the experiments; A. Fursov; V. Fomichev and A. Il'in developed the mathematical modeling and examined the theory validation. The manuscript was written through the contribution of all authors. All authors discussed the results, reviewed, and approved the final version of the manuscript.

Acknowledgments

This research has been supported by the Bulgarian National Science Fund, grant No. KP-06 – Russia/21, the Russian Fundamental research Fund grant No 19-57-18006 and grant No 18-07-01283.

Conflict of Interest

The authors declared no potential conflicts of interest with respect to the research, authorship, and publication of this article.

Funding

This research has been financially supported by the Bulgarian National Science Fund, grant No. KP-06 – Russia/21, the Russian Fundamental research Fund grant No 19-57-18006 and grant No 18-07-01283.

References

[1] Percy, S., Knight, C., McGarry, S., Post, A., Moore, T., Cavanagh, K., *Thermal Energy Harvesting for Application at MEMS Scale*, Springer-Verlag, New York, 2014.

[2] Datas, A., Vaillon, R., Thermionic-enhanced near-field thermophotovoltaics, *Nano Energy*, 61, 2019, 10-17.

[3] Xiong, J., Li, F., Liu, J., Fusion of Different Height Pyroelectric Infrared Sensors for Person Identification, *IEEE Sensors Journal*, 16(2), 2016, 436-446.

[4] Liang, G., Zhou, J., Huang, X., Analytical model of parallel thermoelectric generator, *Applied Energy*, 88(12), 2011, 5193-5199.

[5] Seog, S., Choi, H.J., Kim, S.D., Lee, W.H., Woo, S.K., Han, M.H., Development of alkali metal thermal-to-electric converter unit cells using Mo/TiN electrode, *Journal of the Korean Ceramic Society*, 54(3), 2017, 200-204.

[6] L. Johnson, J. Muller, US Patent, No. US7160639 B2, 2007.

[7] Patterson, D.E, Jamison K.D, Durrett, M., Kashani, A., Gedeon, D., *CVD diamond based miniature stirling cooler*, International cryocooler conference, 2007.

[8] Burugupally, S.P., Weiss, L., Power Generation via Small Length Scale Thermo-Mechanical Systems: Current Status and Challenges, a Review, *Energies,* 11(9), 2018, 2253.

[9] Rosa, R.J., Characteristics of a closed Brayton cycle piston engine, *IEEE Western Canada conference on computer, power and communications systems in a rural environment*, Regina, Sask., Canada, 153–159, 1991.

[10] Pierens, M., Thermeau, J.P, Le Pollès, T., Duthil, P., Experimental characterization of a thermoacoustic travelling-wave refrigerator, *International conference on fluid mechanics, heat transfer and thermodynamics*, Amsterdam, Netherlands, 1057-1061, 2011.

[11] Hussain, M.N, Janajreh, I., Analysis of Pressure Wave Development in a Thermo-acoustic Engine and Sensitivity Study, *Energy Procedia*, 142, 2017, 1488-1495.

[12] Hsu, C-J., Sandoval, S.M., Wetzlar, K.P., Carman, G.P., Thermomagnetic conversion efficiencies for ferromagnetic materials, *Journal of Applied Physics*, 110, 2011,123923–123927.

[13] Bulgrin, K.E., Ju, Y.S., Carman, G.P., Lavine, A.S., A coupled thermal and mechanical model of a thermal energy harvesting device, *ASME 2009 International Mechanical Engineering Congress & Exposition*, Lake Buena Vista, Florida, USA, 327–335, 2009.

[14] Todorov, T., Mitrev, R., Penev, I., Force analysis and kinematic optimization of a fluid valve driven by shape memory alloys, *Reports in Mechanical Engineering*, 1(1), 2020, 61-76.

[15] Webster, J., High integrity adaptive SMA components for gas turbine applications, *Smart Structures and Materials 2006: Industrial and Commercial Applications of Smart Structures Technologies*, San Diego, California, United States, 61710F, 2006.

[16] Song, G., Ma, N., Li, H,. Applications of shape memory alloys in civil structures, *Engineering Structures*, 28, 2006, 1266-1274.

[17] Karimi, S., Konh, B., 3D Steerable Active Surgical Needle, *Design of Medical Devices Conference*, Minneapolis, Minnesota, USA, 1-6, 2019.

[18] Otsuka, K., Wayman, C.M., *Shape memory materials,* Cambridge University Press, Cambridge, 1998.

[19] Schiller, E.H., Heat Engine Driven by Shape Memory Alloys: Prototyping and Design, Master thesis, Virginia Polytechnic Institute and State Univesrity, Blacksburg, VA, 2002.

[20] Jani, J.M., Leary, M., Subic, A., Gibson, M.A., A review of shape memory alloy research, applications and opportunities, *Materials & Design (1980-2015)*, 56, 2014, 1078-1113.

[21] Wang, J., Wu, C., Dai, Y., Zhao, Z., Wang, A., Zhang, T., Wang, Z., Achieving ultrahigh triboelectric charge density for efficient energy harvesting, *Nature Communications,* 88(8), 2017, 1-8.

[22] Deng, H., Du, Y., Wang, Z., Ye, J., Zhang, J., Ma, M., Zhong, X., Poly-stable energy harvesting based on synergetic multistable vibration, *Communications Physics*, 21(2), 2019, 1-10.

[23] Namli, O., Taya, M., Design of piezo-SMA composite for thermal energy harvester under fluctuating temperature, *Journal of Applied Mechanics*, 78(3), 2011, 031001.

[24] Avirovik, D., Kumar, A., Bodnar, R., Priya, S., Remote light energy harvesting and actuation using shape memory alloy-piezoelectric hybrid transducer, *Smart Materials and Structures*, 22(5), 2013, 052001.

[25] Reddy, A., Umapathy, M., Ezhilaras,i D., Uma, G., Piezoelectric Energy Harvester With Shape Memory Alloy Actuator Using Solar Energy, *IEEE Transactions on Sustainable Energy*, 6(4), 1409-1415, 2015.

[26] Todorov, T., Nikolov, N., Todorov, G., Ralev, Y., Modelling and investigation of a hybrid thermal energy harvester, *International Conference on Engineering Vibration (ICoEV 2017), MATEC Web of Conferences 148*, Sofia, Bulgaria, 2018, 1-6.

[27] Marinković, D., Rama, G., Zehn, M., Abaqus implementation of a corotational piezoelectric 3-node shell element with drilling degree of freedom, *Facta Universitatis Series: Mechanical Engineering*, 17(2), 2019, 269 – 283.

[28] Rama, G., Marinković, D., Zehn, M. Efficient three-node finite shell element for linear and geometrically nonlinear analyses of piezoelectric laminated structures, *Journal of Intelligent Material Systems and Structures*, 29(3), 2018, 345–357.

[29] Rama, G., Marinkovic, D., Zehn, M., High performance 3-node shell element for linear and geometrically nonlinear analysis of composite laminates, *Composites Part B: Engineering*, 151, 2018, 118-126.

[30] Noll, M-U., Lentz, L., Wagner, U., On the discretization of a bistable cantilever beam with application to energy harvesting, *Facta Universitatis Series: Mechanical Engineering,* 17(2), 2019, 125 – 139.

[31] Ikuta, K., Tsukamoto, M., Hirose, S., Mathematical model and experimental verification of shape memory alloy for designing micro actuator, *Proceedings of IEEE MEMS*, Nara, Japan, 1991.

[32] Madill, D., David, W., Modeling and L2-Stability of a Shape Memory Alloy Position Control System, *IEEE Transactions on Control Systems Technology*, 6(4), 1998, 473-481.

[33] Donald, J. L., *Engineering analysis of smart material systems*, John Wiley & Sons, Inc, Hoboken, New Jersey, 2007.

[34] Preumont, A., *Mechatronics - Dynamics of Electromechanical and Piezoelectric Systems*, Springer, London, 2006.

[35] Fursov, A.S., Todorov, T.S., Krylov, P.A., Mitrev R.P., On the Existence of Oscillatory Modes in a Nonlinear System with Hystereses, *Differential Equations,* 56, 2020, 1081–1099.

ORCID iD

Rosen Mitrev https://orcid.org/ 0000-0001-6276-1225
Todor Todorov https://orcid.org/0000-0002-6275-476X
Andrei Fursov https://orcid.org/0000-0002-6648-2634
Vasily Fomichev https://orcid.org/0000-0003-2634-3637
Alexander Il'in https://orcid.org/0000-0002-1976-3855

How to cite this article: Mitrev R., Todorov T., Fursov A., Fomichev V., Il'in A. A Case Study of Combined Application of Smart Materials in a Thermal Energy Harvester with Vibrating Action, *J. Appl. Comput. Mech.*, 7(1), 2021, 372–381.
https://doi.org/10.22055/JACM.2020.35128.2571